



1

2 **Measurement report: Long-term variations in carbon monoxide at a**
3 **background station in China's Yangtze River Delta region**

4

5 **Yijing Chen¹, Qianli Ma², Weili Lin^{1,*}, Xiaobin Xu³, Jie Yao², Wei Gao⁴**

6

7

8 ¹College of Life and Environmental Sciences, Minzu University of China, Beijing 100081, China

9 ²Lin'an Atmosphere Background National Observation and Research Station, Lin'an 311307,

10 Hangzhou, China

11 ³Key Laboratory for Atmospheric Chemistry, Chinese academy of meteorological sciences, Beijing

12 100081, China

13 ⁴Shanghai Key Laboratory of Meteorology and Health, Shanghai Meteorological Service, Shanghai

14 200030, China

15 *Corresponding author, email: linwl@muc.edu.cn

16

17

18

19

20

21

22

23

24

25

26

27

28

29



30 **Abstract**

31

32 This study analyzed the long-term variations in carbon monoxide (CO) mixing ratios from January
33 2006 to December 2017 at the Lin'an regional atmospheric background station (LAN; 30.3°N,
34 119.73°E, 138 m a.s.l.) in China's Yangtze River Delta (YRD) region. The CO mixing ratios were
35 at their highest (0.69 ± 0.08 ppm) and lowest (0.54 ± 0.06 ppm) in winter and summer, respectively.
36 The average daily variation of CO exhibited a double-peaked pattern, with peaks in the morning
37 and evening and a valley in the afternoon. A significant downward trend of -11.3 ppb/yr of CO was
38 observed from 2006 to 2017 at the LAN station, which was in accordance with the negative trends
39 of the average CO mixing ratios and total column retrieved from the satellite data (the Measurements
40 Of Pollution In The Troposphere, MOPITT) over the YRD region during the same period. The
41 average annual CO mixing ratio at the LAN station in 2017 was 0.51 ± 0.04 ppm, which was
42 significantly lower than that (0.71 ± 0.12 ppm) in 2006. The decrease in CO levels was largest in
43 autumn (-15.7 ppb/yr), followed by summer (-11.1 ppb/yr), spring (-10.8 ppb/yr), and winter (-9.7
44 ppb/yr). Moreover, the CO levels under relatively polluted conditions (the annually 95th percentiles)
45 declined even more rapidly (-22.4 ppb/yr, $\alpha = 0.05$, $r = -0.68$) from 2006 (0.91 ppm) to 2017 (0.58
46 ppm) and the CO levels under clean conditions (the annually 5th percentiles) were relatively stable
47 throughout the years. The long-term decline and short-term variations in the CO mixing ratios at the
48 LAN station were mainly attributed to the implementation of the anthropogenic pollution control
49 measures in the YRD region and to the events like Shanghai Expo in 2010 and Hangzhou G20 in
50 2016. The decreased CO level may influence atmospheric chemistry over the region. The average
51 OH reactivity of CO at the LAN station is estimated to significantly drop from 4.1 ± 0.7 s⁻¹ in 2006
52 to 3.0 ± 0.3 s⁻¹ in 2017.

53

54 **Keywords:** CO, Long-term trend, Background level, the Yangtze River Delta region

55

56

57

58



59

60 **1. Introduction**

61

62 Carbon monoxide (CO) is a key intermediate in the atmospheric carbon cycle (Novelli et al.,
63 1992). In the troposphere, CO is one of the important air pollutants with high mixing ratios. The
64 volume mixing ratios of CO can reach an order of 10^{-6} (Khalil et al., 1999). CO is also a reactive
65 trace gas that considerably affects health, ecology, and climate, and hence recommended by the
66 Global Atmosphere Watch (GAW) of the World Meteorological Organization (WMO) for priority
67 observation. Fossil fuel combustion (mainly in the northern hemisphere), biomass combustion
68 (mostly in the southern hemisphere), and natural processes (the oxidation of organic compounds,
69 such as methane [CH₄] and isoprene) are the main sources of CO (Holloway et al., 2000; Thompson
70 et al., 1986; Novelli et al., 1998; Andreae and Merlet, 2001; Bakwin et al., 1994). The major sink
71 for CO is its reaction with OH radicals in the troposphere (Holloway et al., 2000; Thompson et al.,
72 1986; Novelli et al., 1998; WMO, 2003). The lifetime of CO in the atmosphere ranges from weeks
73 to months, which makes it an ideal tracer for atmospheric transport processes (Steinfeld and Jeffrey,
74 1998; Worden et al., 2013). Because CH₄ and CO can react with OH radicals (Thompson et al., 1992;
75 Daniel and Solomon, 1998), certain CO mixing ratios can indirectly cause a decrease in CH₄ and an
76 increase in CO₂. Therefore, CO is recognized as an important indirect greenhouse gas. Moreover,
77 CO is an important precursor for the photochemical generation of ozone in a polluted atmosphere
78 (Demerjian et al., 1972).

79 Continuous long-term observation is a method for studying large-scale CO sources, sinks, and
80 long-distance transport. This method allows the CO balance to be determined on a regional or global
81 scale (Fang et al., 2014). In the past decades, many studies have explored the long-term change in
82 CO levels through ground-, aircraft-, or satellite-based observations (Yurganov et al., 2010; Worden
83 et al., 2013; Ahmed et al., 2015; Cohen et al., 2018; Wang et al., 2018). Most of these studies have
84 revealed downward trends for CO concentration. For example, Yurganov et al. (2010) concluded
85 that the CO levels in the Northern Hemisphere decreased from July 2008 to January 2009, mainly
86 due to both the reduction in fossil fuel emissions and the presence of CO-poor air mass transported
87 from tropical regions. Worden et al. (2013) reported that the CO total column over China decreased



88 by $1.6\% \pm 0.5\%/yr$ from 2002 to 2012. Ahmed et al. (2015) analyzed long-term CO observations at
89 two urban sites in Seoul and reported a downward trend of CO from 2004 to 2013. Wang et al. (2018)
90 found that from 1998 to 2014, the total column amount of CO over Beijing and Moscow decreased
91 at $1.14\% \pm 0.87\%/yr$ and $3.73\% \pm 0.39\%/yr$, respectively. Cohen et al. (2018) analyzed the trends
92 of CO in the upper troposphere from 2001 to 2013. In their study, almost all observed trends were
93 negative, with the estimated slopes ranging from -1.37 to -0.59 ppb/yr. The CO data recorded in
94 the Arctic ice core indicated that the CO mixing ratios in this region decreased after the 1970s
95 (Petrenko et al., 2013).

96 Ground-based background measurements are crucial for verifying the accuracy of satellite
97 observation data, reflecting the impact of human activities on air quality and climate change, and
98 evaluating the effectiveness of pollution control measures. In China, many air pollutants have been
99 emitting in very large quantities. For example, the emission of CO was estimated to be about 171
100 Tg in 2010 (Li et al., 2017). To fight against the air pollution, the country has implemented a series
101 of emission control measures in the recent decade. The effectiveness of these measures needs to be
102 verified by observational data, in particular the data from background sites. Long-term background
103 observations over a decade are relatively scarce in China. Reports of long-term background
104 observations of CO are very limited in the literature (Meng et al., 2009; Liu et al., 2019; Zhou et al.,
105 2004; Zhang et al., 2011) and none of them present an analysis of CO variations over a decade. The
106 Yangtze River Delta (YRD) is one of the most developed regions in China. The long-term
107 observation of atmospheric background CO allows for a scientific understanding of the CO source
108 and sink cycle in this region. In this study, we present 12-year (from 2006 to 2017) ground-based
109 observations of CO at a background station in the YRD region. We analyze the long-term CO
110 variations and their determinants in the background areas of eastern China. The results of this study
111 function as scientific evidence for evaluating the effectiveness of pollution control policies and as a
112 reference for formulating practicable air pollution management and emission control measures.

113

114 **2. Monitoring sites and data collection**

115

116 The CO mixing ratios analyzed in this study were collected from January 2006 to December

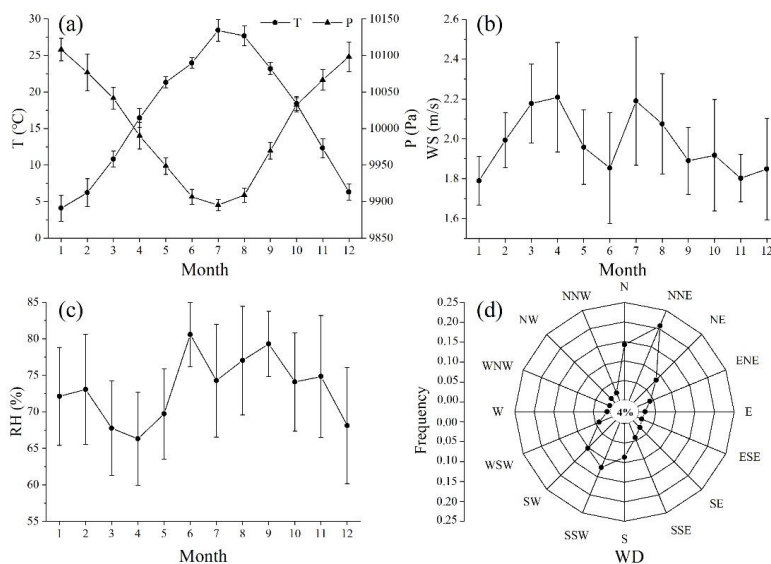


117 2017 at Lin'an (LAN) station (30°25' N, 119°73' E, 138 m asl), a regional atmospheric background
118 monitoring site in China's Zhejiang province. The LAN station is one of the seven atmospheric
119 background stations operated by the China Meteorological Administration, and also a member
120 station of the World Meteorological Organization (WMO) Global Atmosphere Watch (GAW)
121 programme. The measurements at this station reflect the changes in the YRD region's atmospheric
122 background composition (Qi et al., 2012). The LAN station is located approximately 50 km west of
123 Hangzhou (the capital city of Zhejiang province) and 150 km southwest of Shanghai. It is influenced
124 by a typical subtropical monsoon climate. Fig. 1 displays the seasonal variations in air temperature
125 (T), wind speed (WS), pressure (P), and relative humidity (RH) as well as the wind direction (WD)
126 frequency at the LAN station from 2006 to 2017. These data were obtained from the regular
127 meteorological observations at the LAN station. As displayed in Fig. 1, the seasonal temperature
128 trend at the LAN station was of a convex shape. The highest and lowest temperatures occurred in
129 July (28.4°C) and January (4.1°C), respectively. In opposition to the seasonal change in temperature,
130 the seasonal change in atmospheric pressure at the LAN station showed a concave shape, with the
131 lowest and highest pressures occurring in July (989.51 hPa) and January (1010.81 hPa), respectively.
132 The seasonal patterns of the WS and RH at the LAN station were not as clear as those of air
133 temperature and pressure. The seasonal average WS was lowest in winter (1.9 m/s) and highest in
134 spring (2.1 m/s). The RH was highest in summer (77%) and lowest in spring (68%). The winds at
135 the LAN station mostly originated from the northeast and southwest, as shown in Fig. 1d. On
136 average, the northeast and southwest winds accounted for 29.2% and 22.6% of the winds,
137 respectively. The calm wind frequency was 4%.

138 A gas-filter correlation infrared absorption analyzer (48C trace level, Thermo Fisher, USA)
139 was used to measure the surface CO mixing ratios. The analyzer has a limit of detection of 0.04
140 ppm. Infrared radiation is chopped and passed through a rotating gas-filter lens, a one half of which
141 is filled with CO and the other with nitrogen. Thus, reference and measurement beams are produced
142 in alternation. The beams then pass through a narrow-band interference filter and sample cell.
143 Because the CO in the sample cell can only absorb the measurement beam, and the other gases can
144 absorb both beams, the measurement signal of CO could be obtained by comparing the attenuation
145 intensity between the reference and measurement beams.



146 The measurement signal from the CO analyzer was recorded every 5 min. Zero check and span
147 check were conducted every 6 and 24 hours, respectively. Multipoint (>5) calibration was performed
148 once a month using standard CO gas mixture (CO in nitrogen). Because the zero point of the
149 instrument drifted with time, we performed linear interpolation between two adjacent zero checks
150 to obtain the zero signals for given time point between the zero checks. These zero signals were
151 used in the corrections of the CO data. We performed response correction according to the results
152 of multipoint calibrations as well as the zero and span checks (Lin et al., 2009). Finally, we corrected
153 the data according to the quantity transfer and traceability results (Lin et al., 2011). Valid 5-minute
154 data were used to calculate the hourly mean mixing ratios. At least 10 data points were required for
155 any given hour to calculate that hour's mixing ratio. Missing data were caused by the malfunction
156 of the instrument from February 1 to 13, 2007, and from abnormal measurement fluctuations from
157 May 30 to July 17, 2009.



158 **Fig. 1.** Seasonal variations in (a) temperature, (b) WS, (c) air pressure, (d) RH, and (e) WD
159 frequency distribution (the static wind frequency was 4%) at the LAN station from 2006 to 2017
160 (an error bar represents one standard deviation)

161
162



163 **3. Results and discussion**

164

165 **3.1 Observed levels and comparisons with other sites**

166 Fig. 2 displays the time series of hourly mean CO levels at the LAN station from January 1,
167 2006, to December 31, 2017 and the linear fitting results of the hourly mean CO mixing ratios. The
168 overall mean (\pm one standard deviation) and median values of the CO mixing ratios in the
169 aforementioned 10 years were $0.62 (\pm 0.23)$ ppm and 0.57 ppm, respectively. The highest (2.98 ppm)
170 and lowest (0.08 ppm) hourly mean mixing ratios occurred at 17:00 on January 10, 2008, and 18:00
171 on October 4, 2007, respectively. The highest hourly mean CO mixing ratio was considerably lower
172 than the second-level hourly limit (approximately 8 ppm) of the ambient air quality standard in
173 China (GB 3095-2012). The highest (2.38 ppm) and lowest (0.23 ppm) daily mean mixing ratios
174 occurred on January 10, 2008, and August 31, 2011, respectively. The highest daily mean value was
175 also below the daily limit for air quality standard (3.2 ppm). The lowest monthly average CO
176 concentration was 0.39 ppm on August 2011, and the highest concentration was 1.00 ppm on
177 January 2010. The median of daily mean CO levels from January 2006 to December 2017 was 0.58
178 ppm. The overall CO concentrations at the LAN were much higher than those observed at the
179 Waliguan global baseline station from 2006-2017 and some regional background stations outside
180 China (Table 1), indicating that East China has been one of the regions with high CO levels.

181

182

183

184

185

186

187

188

189

190

191 **Fig. 2.** Time series of the CO variations at the LAN station from 2006 to 2017

192

193

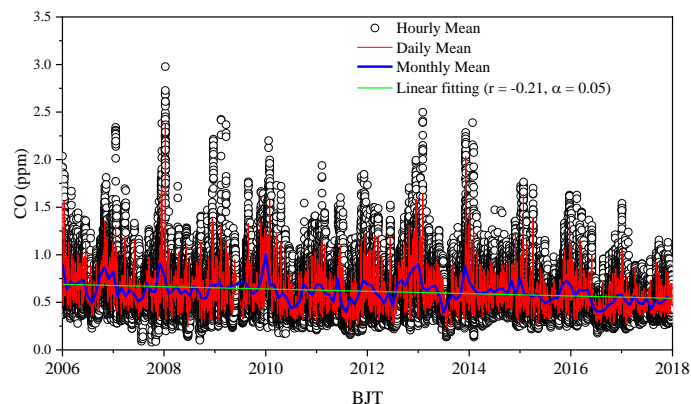




Table 1. Comparison of seasonal average CO variations at the LAN station and other similar background stations around the world

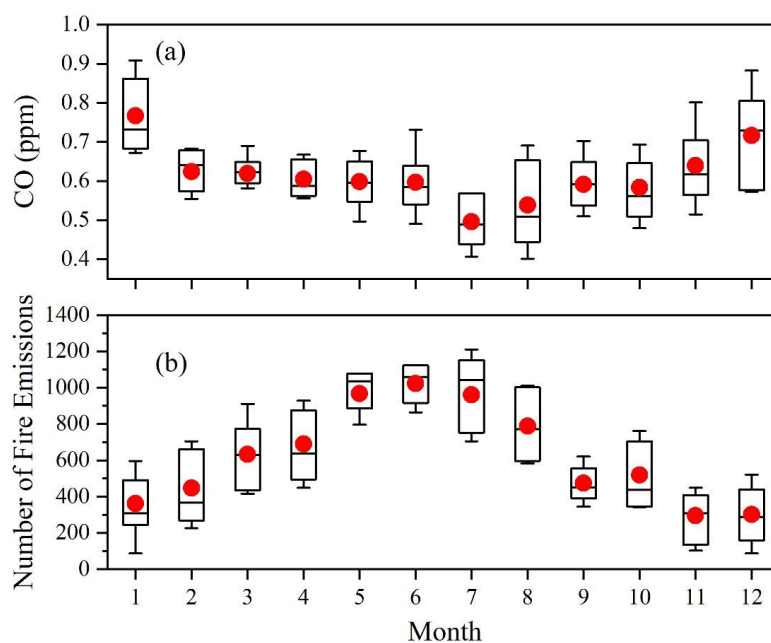
Site	Location	Period				Trends (ppb/yr)	Ref.	
		Spring (ppm)	Summer (ppm)	Autumn (ppm)	Winter (ppm)			
Lin'an, China	30°18'N, 119°44'E, 138 m	2006~2009	0.65 ± 0.04	0.59 ± 0.04	0.65 ± 0.08	0.75 ± 0.05	-11.3	This study
		2010~2015	0.59 ± 0.04	0.54 ± 0.06	0.62 ± 0.07	0.70 ± 0.07		
		2016~2017	0.57 ± 0.08	0.46 ± 0.04	0.49 ± 0.03	0.56 ± 0.01		
Lin'an, China	30°18'N, 119°44'E, 189 m	2010/9~2012/2	0.47 ± 0.01	0.30 ± 0.01	0.41 ± 0.00	0.52 ± 0.01	-	Fang et al., 2014
Lin'an, China	30°18'N, 119°44'E, 189 m	2010/9~2017/5	0.38 ± 0.00	0.28 ± 0.00	0.37 ± 0.00	0.45 ± 0.00	-16.3	Liu et al., 2019
Shangdianzi, China	40°39'N, 117°07'E, 293 m	2006/1~2006/12	0.75 ± 0.16	0.64 ± 0.14	0.80 ± 0.12	0.76 ± 0.13	-	Meng et al., 2009
Shangdianzi, China	40°39'N, 117°07'E, 293 m	2011/12~2017/5	0.16 ± 0.00	0.18 ± 0.00	0.14 ± 0.00	0.16 ± 0.00	-1.3	Liu et al., 2019
Longfengshan, China	44°44'N, 127°36'E, 311 m	2006	0.21	0.20	0.27	0.38	-	Wu et al., 2008
Jinsha, China	29°38'N, 114°12'E, 750 m	2006/6~2007/7	0.44	0.39	0.66	0.60	-	(Lin et al., 2011)
Waliguan, China	36°28'N, 100°89'E, 3810 m	2006/1~2017/12	0.13 ± 0.01	0.13 ± 0.01	0.12 ± 0.01	0.12 ± 0.01	-0.67	WDCGG
Tae-ahn Peninsula, Korea	36.73°N, 126.13°E, 20 m	2006/1~2017/12	0.27 ± 0.03	0.19 ± 0.04	0.21 ± 0.03	0.23 ± 0.02	-0.43	WDCGG
Yonagunijima, Japan	24.47°N, 123.01°E, 30 m	2006/1~2017/12	0.18 ± 0.03	0.09 ± 0.01	0.13 ± 0.02	0.19 ± 0.02	-0.98	WDCGG
Park Falls (WD), the U.S.	45.93°N, 90.27°W, 868 m	2006/1~2017/12	0.17 ± 0.02	0.16 ± 0.03	0.14 ± 0.02	0.16 ± 0.02	-0.96	WDCGG
Payerne, Switzerland	46.81°N, 6.94°W, 490 m	2006/1~2017/12	0.20 ± 0.04	0.14 ± 0.01	0.20 ± 0.04	0.28 ± 0.05	-5.20	WDCGG

194
 195
 196
 197
 198
 199
 200
 201
 202
 203
 204
 205
 206
 207
 208
 209
 210
 211
 212
 213
 214
 215
 216
 217
 218
 219
 220
 221
 222
 223
 224
 225
 226
 227
 228
 229
 230
 231
 232
 233
 234
 235
 236
 237



238 3.2 Seasonal variation

239 Fig. 3 shows the seasonal variations in CO mixing ratios at the LAN station and the number of
240 fire emissions (retrieved from the Global Fire Emissions Database version 4 described in Werf
241 et al., 2017) in the YRD region (22°N~40°N, 112°E~123°E) from 2006 to 2017.



242
243 **Fig. 3.** Seasonal variations in CO mixing ratios at the LAN station and the number of fire emissions
244 in the YRD region from 2006 to 2017. The lines and dots in the box are the median and mean
245 concentrations, respectively, the box's lower and upper limits represent 25th and 75th percentiles
246 concentrations range, respectively, and the lower and upper whiskers correspond the 10th and 90th
247 percentiles values.

248 As can be seen in Fig. 3(a), the average CO mixing ratios were the highest in the winter (0.69
249 ± 0.08 ppm), followed by the spring (0.61 ± 0.05 ppm), autumn (0.61 ± 0.09 ppm), and summer
250 (0.54 ± 0.06 ppm). In the winter, because of the weak radiation, the photochemical consumption of
251 CO in the atmosphere decreased. Also, the atmospheric stability was high and the diffusion
252 conditions were unfavorable. Therefore, atmospheric CO accumulated easily and reached its
253 maximum concentration in the winter. Nevertheless, the photochemical reaction was strong in the



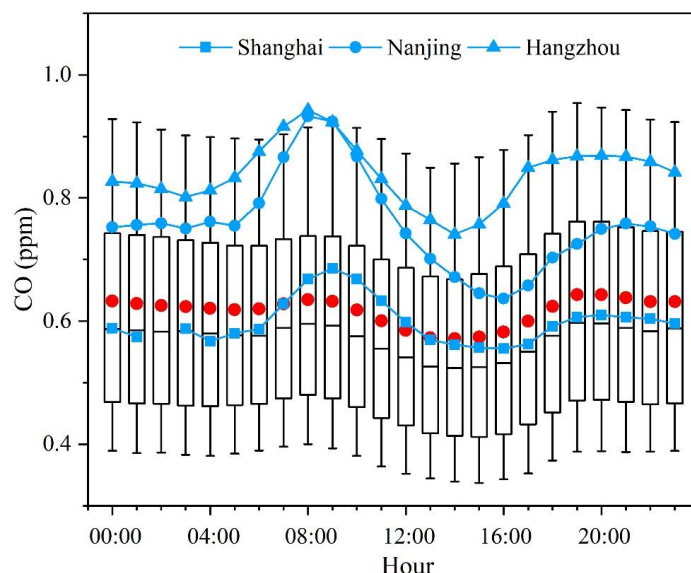
254 summer, which resulted in an increase in the mixing ratios of OH radicals and the chemical
255 consumption of atmospheric CO. Moreover, the boundary layer height was relatively high in the
256 summertime, which promoted the vertical diffusion and dilution of CO in the atmosphere. Therefore,
257 the CO mixing ratios were the lowest in the summer. By contrast, the seasonal variations in the
258 number of fire emissions in the YRD region (Fig.3b) were opposite to the trend of the CO mixing
259 ratios in different months, which indicated that open fire burning was not a main factor affecting the
260 atmospheric CO concentrations at the LAN station from 2006 to 2017.

261 **3.3 Diurnal variation**

262 The daily variations in the CO mixing ratios were influenced by emission sources, atmospheric
263 transport (horizontal and vertical), and the evolution of the atmospheric boundary layer (Xue et al.,
264 2006). Fig. 4 displays the average daily variations in the CO mixing ratios at the LAN station, along
265 with those cities Shanghai, Nanjing and Hangzhou. As displayed in Fig. 4, the CO mixing ratios
266 exhibited double peaks, with higher CO levels in the morning and evening but lower CO levels in
267 the afternoon. The peak of the CO mixing ratios at the LAN station mostly occurred in the morning
268 (7:00–10:00) and at night (19:00–24:00). The lowest CO mixing ratios were observed between
269 12:00 and 16:00. The hourly CO mixing ratios usually reached their minimum value in the afternoon
270 due to the high atmospheric boundary layer, intense vertical diffusion mixing, and sufficient OH
271 radicals at that time. The peak CO mixing ratios at the LAN station occurred during the morning
272 and evening rush hours. This is consistent with those observed in the urban areas of Shanghai (Gao
273 et al., 2017), Nanjing (Huang et al., 2013a), and Hangzhou (Zhang et al., 2018) (Fig. 4). Thus, the
274 CO mixing ratios at the LAN station were affected by the pollutant emissions related to
275 transportation in the surroundings. However, the peak-valley difference of CO at LAN was much
276 smaller than those found in the cities, reflecting reduced impacts from direct emissions on this
277 background site.



278



279 **Fig. 4.** Diurnal variations in CO mixing ratios at Shanghai, Nanjing, Hangzhou, and the LAN station
280 from 2006 to 2017. The lines and red dots in the box are the median and mean CO concentrations
281 at the LAN station, respectively, the box's lower and upper limits represent 25th and 75th percentiles
282 concentrations, respectively, and the lower and upper whiskers correspond the 10th and 90th
283 percentiles values.

284

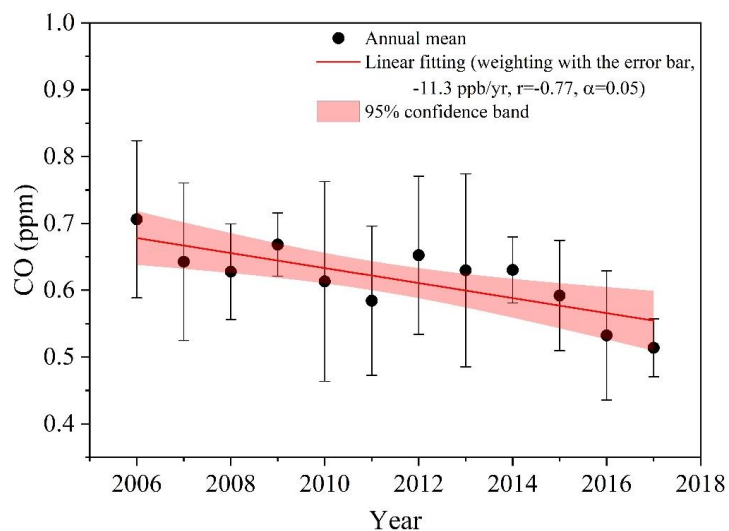
285 3.4 Long-term trends

286 3.4.1 Trends of annual means

287 Fig. 5 shows the change in the annual mean CO mixing ratios at the LAN station from 2006 to
288 2017. The CO levels varied across the years. The World Expo was held in Shanghai from May to
289 October 2010, when air pollution prevention and control measures were strengthened in Shanghai
290 and its surrounding areas. Because of these strengthened measures, the number of days with good
291 air quality reached its highest value since 2001 (Huang et al., 2013b). Fig. 5 also indicates that the
292 average CO mixing ratio in 2010 was lower than those from 2006 to 2009 (1.5 months of data were
293 missing for the summer of 2009). The CO level continued to decline in 2011 but increased in 2012,
294 after which the CO level decreased steadily. China officially implemented the Action Plan for The
295 Prevention and Control of Air Pollution in 2013, which comprehensively intensified air pollution
296 control efforts and reduced multi-pollutant emissions. The plan called for 5-year efforts to improve



297 overall air quality and significantly reduce heavy pollution. As illustrated in Fig. 5, the effects of the
298 aforementioned action plan began to be observed in 2014, and the CO mixing ratios started to
299 decline significantly. Overall, the annual average of CO at LAN showed a decrease trend of 11.3
300 ppb/yr ($\alpha = 0.05$) during 2006-2017. For the period 2010-2017, we obtained a trend of -14 ppb/yr
301 ($\alpha = 0.05$). This rate of decline in the CO mixing ratio was slightly lower than that (-16.3 ppb/yr)
302 reported by Liu et al. (2019) for the same station for 2010-2017. The measurements of Liu et al.
303 (2019) were performed using a cavity ring-down spectrometer, their air samples were drawn from
304 a tower (intake height: 50 m agl), and their trend was based on non-linear fitting on CO values after
305 removing those impacted by local events. The CO decreasing trend obtained in this study is smaller
306 than those reported by Ahmed et al. (2015) with values of -20 ppb/yr and -13 ppb/yr respectively
307 for two urban sites in South Korea during 2004–2013, larger than that reported by Liu et al. (2019)
308 with a value of -1.3 ppb/yr for a regional atmospheric background station in northern China during
309 2011–2017, and about a factor of 2-26 of those found in regional atmospheric background stations
310 in Korea, Japan, and Switzerland (Table 1).
311

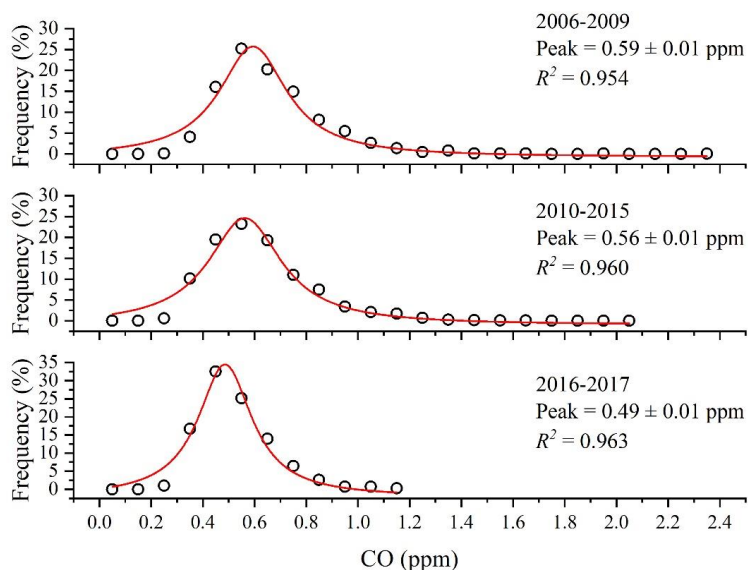


312
313 **Fig. 5.** Variation in the annual mean CO mixing ratios at the LAN station from 2006 to 2017 (the
314 error bars represent one standard deviation)

315 Considering the variation trend in Fig. 5 and the major air pollution control policies adopted
316 during the study period, we divided the study data into three subsets of data (collected during 2006–
317 2009, 2010–2015, and 2016–2017, respectively). The frequency distributions of average daily CO



318 mixing ratios in the three data subsets and the Lorentz curve fitting results are displayed in Fig. 6.
319 Approximately, a unimodal structure of CO frequency distribution was observed for all the datasets.
320 The peak values of the Lorentz curves can be used to characterize the background concentration
321 levels of atmospheric pollutants for a specific time and region (Lin et al., 2011). The peak of the CO
322 Lorentz curve shifted towards lower mixing ratios over time and the trailing phenomenon of the
323 fitting curve diminished gradually. The peak concentration of the fitting curve was 0.59 ± 0.01 ppm
324 from 2006 to 2009. During 2010–2015 and 2016–2017, the peak CO concentrations were $0.56 \pm$
325 0.01 and 0.49 ± 0.01 ppm, respectively. The peak frequency of the Lorentz curve was higher in
326 2016–2017 than in 2006–2015. Moreover, the peak width was significantly narrower in 2016–2017
327 than in 2006–2015. These are resulted from a decrease over time in the regional background mixing
328 ratios of CO.
329



330
331 **Fig. 6.** Frequency distribution of the CO mixing ratios and Lorentz curve fitting results for
332 different time intervals

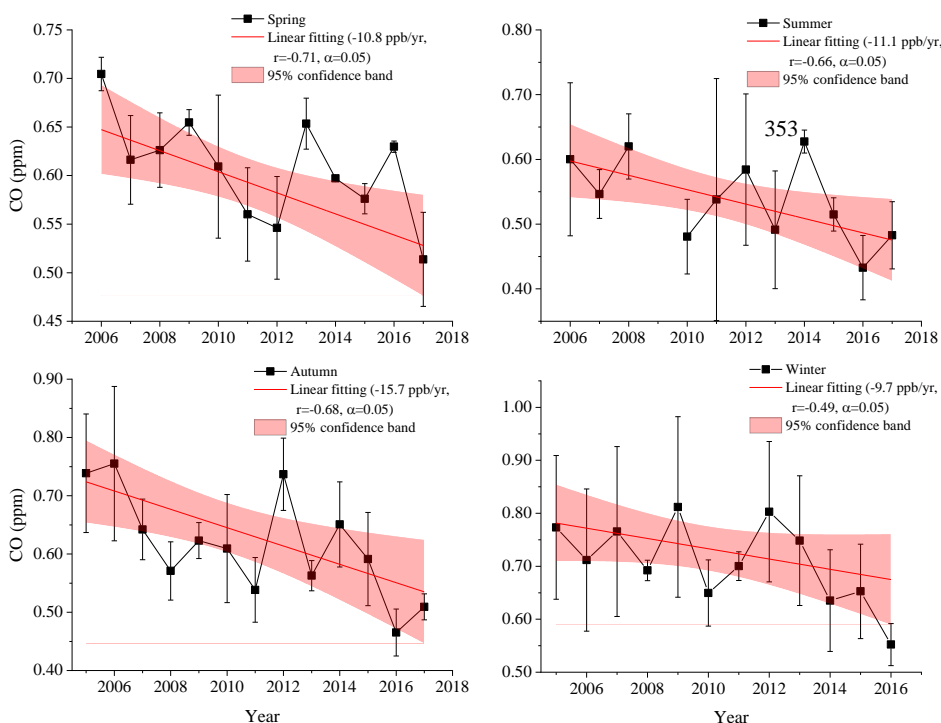
333 3.4.2 Trends of seasonal means

334 The time series of seasonal average levels of CO at the LAN station from 2006 to 2017 are
335 displayed in Fig. 7. Linear trends were calculated from the seasonal data, with standard errors being
336 used as weighting factors. From 2006 to 2017, the seasonal CO mixing ratios exhibited larger



337 fluctuations; nevertheless, an overall significant ($\alpha = 0.05$) decreasing trend was observed in each
338 season. The largest decrease (the slope of linear fitting) in the seasonal CO levels occurred in autumn
339 (-15.7 ppb/yr), followed by summer (-11.1 ppb/yr), spring (-10.8 ppb/yr), and winter (-9.7 ppb/yr).

340 Table 1 presents a comparison of the seasonal average CO mixing ratios at the LAN station
341 and other background stations in the world from 2006 to 2017. As indicated in Table 1, the CO
342 mixing ratios at the LAN station in the four seasons between 2016 and 2017 were lower than those
343 between 2006 and 2015, with the largest decrease of 0.19 ppm occurring in winter. The seasonal
344 CO mixing ratios at the LAN station were marginally lower than those at the Shangdianzi station in
345 northern China (Meng et al., 2009), but were almost 3 times higher than those at many other regional
346 atmospheric background stations outside China, such as the Tae-ahn Peninsula station in Korea,
347 Yonagunijima station in Japan, Park Falls (WI) station in the U.S., and Payerne station in
348 Switzerland from 2006 to 2017 (Table 1). Moreover, the CO mixing values observed at the LAN
349 station were nearly 5 times higher than those observed at the Waliguan station, a global baseline
350 station in China. In conclusion, the CO levels at the LAN station were relatively high compared to
351 other regional atmospheric background stations outside China because of more intense
352 anthropogenic emissions in the YRD region.



354

355 **Fig. 7.** Seasonal time series and linear fitting of CO mixing ratios at the LAN station

356 (Spring: March to May, Summer: June to August, Autumn: September to November, and Winter:

357 December to February)

358

359 3.4.3 Trends of CO levels under clean and polluted condition

360 In the annual statistics, the 95th and 5th percentiles of the CO mixing ratios can be viewed as

361 the CO levels in the most polluted and clean (background) airmasses, respectively. Here, we use

362 these two quantities to study CO trends under polluted and clean conditions, respectively, at the

363 LAN station. As illustrated in Fig. 8 (a), the CO concentration under the polluted condition

364 experienced an significant decreasing trend of -22.4 ppb/yr ($\alpha = 0.05$, $r = -0.68$) from 2006 (0.91

365 ppm) to 2017 (0.58 ppm) and that under the clean condition was relative stable (no significant trend)

366 throughout the years. This suggests that the CO levels in pollution plumes, which are highly

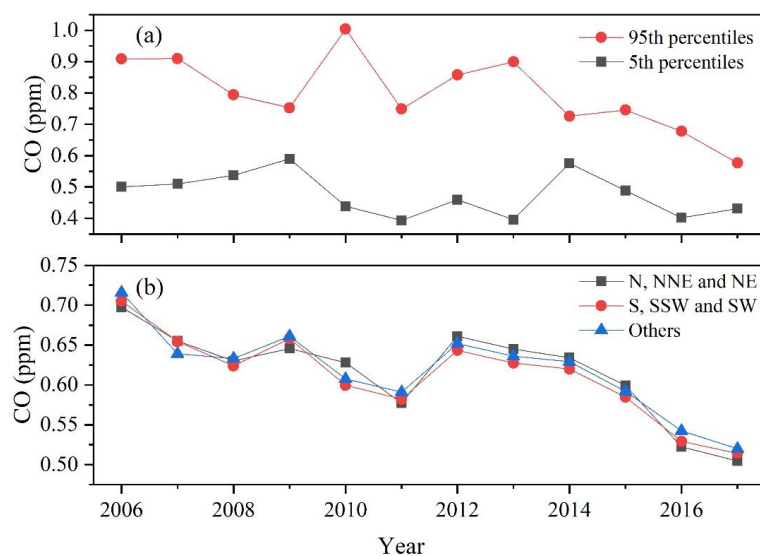
367 impacted by anthropogenic emissions in the YRD region, have been reduced greatly, while the

368 background levels of CO at the LAN station have not changed much. Fig. 8 (b) shows the average

369 CO concentrations from prevailing (N, NNE, NE, S, SSW and SW) and other wind directions. As



370 can be seen in Fig. 8 (b), the annual CO levels from different wind directions generally presented
371 similar patterns and all of them exhibited a significant ($\alpha = 0.05$) downward trend, suggesting that
372 the CO concentrations in the provinces and cities surrounding the LAN station have all decreased.



373

374 **Fig. 8.** Trends of CO mixing ratios at 95th and 5th percentiles and from different wind directions

375

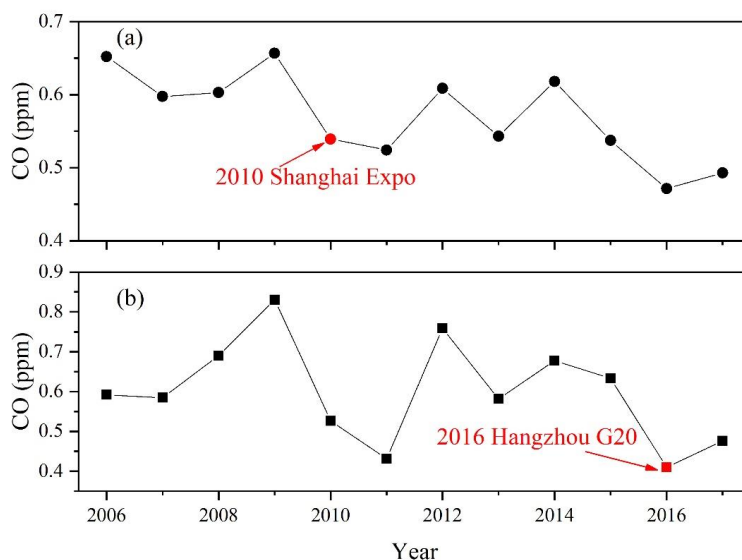
376 3.5 Causes and implications of the long-term variations

377 3.5.1 Impacts of Shanghai Expo and G20 in Hangzhou

378 During the Shanghai Expo in 2010 (from 1 May to 31 October) and Hangzhou G20 in 2016
379 (from 24 July to 6 September), the Chinese government has implemented a series of joint pollution
380 control measures in the cities of the YRD region to ensure good air quality during these mega-events.
381 A satellite-based study (Hao et al., 2011) reported that a 12% reduction of CO concentration was
382 observed over Shanghai city during the Expo compared to the past three years. Zhang et al. (2017)
383 found that the ground CO levels in Hangzhou city decreased by 56% during G20 as opposed to
384 those in 2015. In order to further evaluate the effect of these control strategies, we compared the
385 annual trends of CO concentrations at the LAN station during the same period of Shanghai Expo
386 and Hangzhou G20, which are shown in Fig. 9 (a) and (b), respectively. The concentration of CO at
387 the LAN station was 0.54 ppm during the Expo and 0.41 ppm during the G20, and the values were
388 lower than those observed in Shanghai city (0.86 ppm) and Hangzhou city (0.53 ppm) in the same
389 period. Sharp decreases (reductions of 18 % during the Expo in 2010 and 35% during the G20 in
390 2016) of the CO mixing ratios were observed at the LAN station compared to those during the same



391 periods in the previous years, indicating that the pollution control measures worked well so as to
392 reduce atmospheric CO concentrations in the YRD region.



393

394 **Fig. 9.** Average CO levels for the periods corresponding to (a) 2010 Shanghai Expo (from 1 May
395 to 31 October) and (b) 2016 Hangzhou G20 (from 24 July to 6 September)

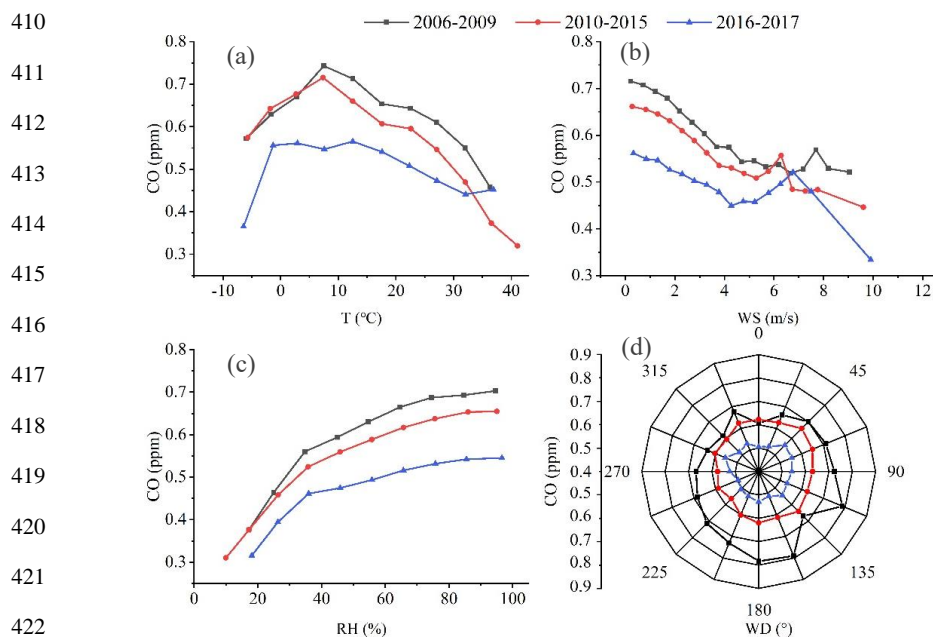
396

397

398 3.5.2 Relationships with meteorological conditions

399

Atmospheric CO mixing ratios are not only affected by local emission sources and the mixing
400 ratios of atmospheric OH radicals but also by meteorological conditions. Temperature, WS, WD,
401 and other meteorological conditions directly affect atmospheric stability and photochemical reaction
402 intensity, which influence the transmission capacity, generation, consumption rate, and lifetime of
403 atmospheric CO diffusion (Steinfeld and Jeffrey, 1998). Meteorological conditions varied across the
404 years of our study period. Such variations affected the comparison of the atmospheric CO mixing
405 ratios between different time intervals, especially when analyzing or evaluating the effectiveness of
406 pollution control policies. To minimize the effects of meteorological conditions on the analysis
407 results, we took temperature, WS, and WD as classification variables and analyzed the variation in
408 the CO mixing ratios under similar meteorological conditions during the three periods. The results
409 are displayed in Fig. 10.



410
411
412
413
414
415
416
417
418
419
420
421
422
423 **Fig. 10.** Variations of CO mixing ratios in different periods with respect to temperature, WS, RH,
424 and WD

425 As displayed in Fig. 10(a), the plot of the CO mixing ratios versus the temperature had a convex
426 shape, with relatively low concentrations occurring at both high and low temperatures. Generally,
427 because the photochemical reaction of CO intensifies at extremely high temperatures, and strong
428 winds occur at extremely low temperatures, both high temperatures and strong winds can cause low
429 CO mixing ratios. The decrease in the CO mixing ratios in a relatively high-temperature range
430 during 2016—2017 was lower than the corresponding decreases in previous years. This result might
431 be attributable to the summertime increase in energy consumption from the widespread use of air
432 conditioners in China. Compared with 2006—2015, the stable area with high CO mixing ratios
433 started to appear at lower temperatures during 2016—2017, which reflected the effectiveness of
434 pollution control measures on the large emission sources. As displayed in Fig. 10(b), as the WS
435 increased within a given range, the CO mixing ratios gradually decreased because of the
436 strengthened diffusion and dilution of the atmosphere. When WS increased to a given level, where
437 this level differed between the time intervals and continually decreased overtime, the CO mixing
438 ratios increased with WS. This may be attributable to the pollution sources being increasingly close



439 to the LAN station because of increased urbanization over time. At a WS of 6–7 m/s, the CO mixing
440 ratios in the different time intervals tended to be consistent. As the WS continued to increase to
441 approximately 8 m/s, the atmospheric CO mixing ratios significantly decreased with the WS. As
442 displayed in Fig. 10(c), the CO mixing ratios correlated positively with RH, which is consistent with
443 the results reported by Turkoglu et al. (2004) and Ye et al. (2008). The main sink of CO is the
444 oxidation reaction with OH radicals (Steinfeld and Jeffrey, 1998). Because water vapor is a
445 precursor of clouds, at higher levels of RH, the atmosphere is more likely to be oversaturated with
446 water and form clouds, and, because clouds can reflect sunlight and reduce the ultraviolet radiation
447 reaching the ground, the photochemical reaction between CO and OH radicals is weakened (Ye., et
448 al., 2008). Fig. 10(d) displayed the change in CO mixing ratios with respect to WD. The figure
449 indicates that CO levels were the highest in the south sector of the LAN station.

450 Table 2 summarized the average percentage decrease in the CO mixing ratios during 2010–
451 2015 and 2016–2017 relative to CO mixing ratios in the previous time intervals under the same
452 meteorological conditions (temperature, WS, RH, and WD). As indicated in Fig. 10 and Table 2, the
453 CO mixing ratios during 2016–2017 were generally lower than those during 2006–2009 and 2010–
454 2015.

455
456 **Table 2.** Comparison of the average percentage decline in CO mixing ratios during 2010–2015
457 and 2016–2017 relative to CO mixing ratios in previous time intervals under the same
458 meteorological factors

	Decreased Percentage (%)			
	T	WS	RH	WD
2010-2015*	-6.2	-13.6	-9.6	-11.9
2016-2017**	-14.5	-10.7	-11.7	-14.2
2016-2017*	-19.8	-16.5	-20.4	-24.4

459 *: compared with 2006–2009, **: compared with 2010–2015.

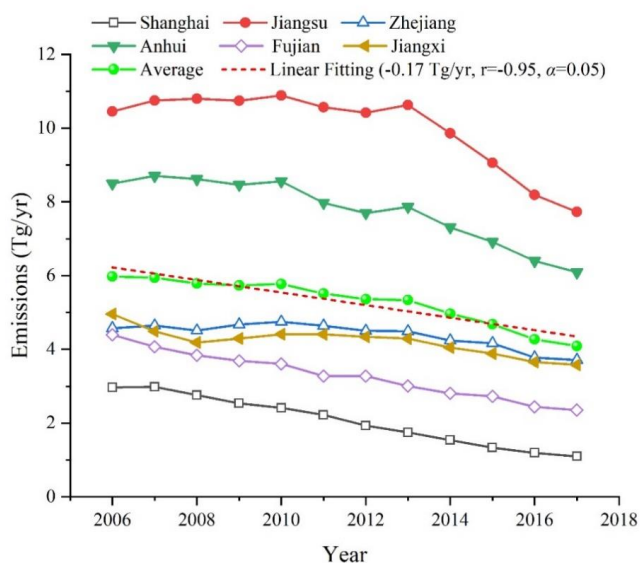
460

461 3.5.3 Changes in emissions in neighboring provinces

462 China has implemented a comprehensive energy conservation and emission reduction policy
463 since 2006 (Zhao et al., 2008; Lei et al., 2011). Small and old factories and boilers have been



464 gradually replaced by larger and more energy-efficient alternatives. Although the focus of these
465 measures was to control sulfur dioxide emissions, these measures also greatly improved combustion
466 efficiency and thus decreased CO emissions (Zhao et al., 2012). Fig. 11 displayed the change in the
467 CO emissions in six provinces and cities around the LAN station from 2006 to 2017. The emission
468 data were obtained from the Multiresolution Emission Inventory for China (Li et al., 2017). As
469 indicated in Fig. 11, the average annual CO emissions of the provinces and cities surrounding the
470 LAN station declined significantly ($\alpha = 0.05$, $r = -0.95$), With an average decline rate of 170,000
471 tons/yr. The percentages of CO emission decreased during 2016–2017 in Shanghai city as well as
472 Jiangsu, Zhejiang, Anhui, Fujian, and Jiangxi provinces were -59.3% , -25.5% , -18.6% , -27.2% ,
473 -40.1% , and -19.3% , respectively, relative to CO emission values during 2006–2009. In summary,
474 the decline in the CO mixing ratios at LAN station was mainly caused by the reduction of
475 anthropogenic CO emissions in its surrounding areas due to the effectiveness of the adopted
476 pollution control measures.



477
478 **Fig. 11.** CO emissions from 2006 to 2017 in the provinces and cities surrounding LAN station and
479 linear fitting of the average annual CO emissions of the six provinces and cities

480 Data source: <http://meicmodel.org/dataset-mix.html>

481 3.5.4 Implications on regional atmospheric chemistry



482 The tropospheric CO has been measured on a global scale from the Measurements Of Pollution
483 In The Troposphere (MOPITT) instrument on the spacecraft since 2000 (Deeter et al., 2017).
484 Monthly CO mixing ratios at the surface layer and the CO total column concentrations over the
485 YRD region from 2006 to 2017 were retrieved from MOPITT (MOP02J Version 8, 2018;
486 http://www.satdatafresh.com/CO_MOPITT.html). From 2006 to 2017, the average CO mixing ratio
487 from MOPITT over the YRD region (22.5°N~39.5°N, 112.5°E~123.5°E) in 2006 (0.11 ± 0.02 ppm)
488 was higher than those in 2017 (0.10 ± 0.02 ppm), with a significant declining trend of -0.5 ppb/yr
489 ($\alpha = 0.05$, $r = -0.82$). As for the average CO total column, the value in 2006 ($1.91 \times 10^{18} \pm 0.23$
490 $\times 10^{18}$ molecules/cm²) was also higher than those in 2017 ($1.76 \times 10^{18} \pm 0.21 \times 10^{18}$
491 molecules/cm²), with a significant declining trend of -1.07×10^{16} molecules/(cm²·yr) ($\alpha = 0.05$, $r =$
492 -0.70) from 2006 to 2017. They are in consistent with the negative trends of the aforementioned
493 ground CO levels measured in the sites of the WDCGG network (Table 1) and at the LAN station.

494 The major sink for CO is reaction with OH radical (Steinfeld and Pandis, 2006), so a decrease
495 in the CO concentrations may lead to an increase in the lifetime of OH radical and thus affect the
496 atmospheric OH photochemistry (i.e., ozone production). The lifetime of OH is defined as the
497 inverse of the OH reactivity (i.e., OH loss rates), and the total OH reactivity is calculated by summing
498 over all the products of the OH reactants (CO, volatile organic compounds, nitrogen oxides, etc.)
499 concentrations times their respective rate coefficients with OH (k_{OH}) (Kovacs and Brune, 2001; Di
500 Carlo et al., 2004). The lowest average total OH reactivity ($5 \text{ s}^{-1} \sim 6 \text{ s}^{-1}$) observed in the rural areas
501 around the world (Ren et al., 2005; Ingham et al., 2009). The k_{OH} of CO is 350 /(ppm·min) at the
502 standard temperature of 298K (Vukovich, 2000) and CO generally contributed 10%~20% to the
503 total OH reactivity at the rural sites of China (Lou et al., 2009). From 2006 to 2017, the average OH
504 reactivity of CO at the LAN station exhibited a significant downward trend of $-0.07 \text{ s}^{-1}/\text{yr}$ ($\alpha = 0.05$,
505 $r = -0.80$) and the average monthly OH reactivity of CO dropped from $4.1 \pm 0.7 \text{ s}^{-1}$ in 2006 to 3.0
506 $\pm 0.3 \text{ s}^{-1}$ in 2017.

507

508 4. Conclusion

509 The average annual levels of CO at the LAN station during 2006–2009, 2010–2015, and 2016–
510 2017 were 0.66 ± 0.03 ppm, 0.62 ± 0.03 ppm, and 0.52 ± 0.01 ppm, respectively. From a seasonal



511 perspective, the highest seasonal average CO mixing ratio occurred in winter (0.69 ± 0.08 ppm),
512 followed by spring (0.61 ± 0.05 ppm), autumn (0.61 ± 0.09 ppm), and summer (0.54 ± 0.06 ppm).
513 The average daily variations in the CO concentration exhibited a double-peaked pattern, with high
514 CO concentrations in the morning and evening and low CO concentrations in the afternoon. Such
515 diurnal variations suggest that the CO mixing ratios at the LAN station were affected by traffic
516 pollutant emissions in its surrounding area.

517 The average annual atmospheric CO mixing ratios at the LAN station exhibited a significant
518 decreasing trend (-11.3 ppb/yr, $\alpha = 0.05$) from 2006 to 2017, which was consistent with the negative
519 trends of the average CO mixing ratios and total column retrieved from MOPITT over the YRD
520 region. The measurements at the LAN station well reflected regional changes in atmospheric
521 background CO mixing ratios in the YRD region. The largest decrease in the CO level was observed
522 in autumn (-15.7 ppb/yr), followed by summer (-11.1 ppb/yr), spring (-10.8 ppb/yr), and winter ($-$
523 9.7 ppb/yr). The significant downward trend of the CO mixing ratios at the LAN station was not
524 caused by meteorological conditions but by strengthened pollution control measures, which
525 indicated that the adopted measures were effective. In spite of the nearly a quarter of reduction
526 during 2006-2017, the CO levels at the LAN station were still much higher those at other regional
527 atmospheric background stations around the world so that further reductions in CO emissions in the
528 YRD region are needed. The significant decrease of regional CO level has an implication for
529 atmospheric chemistry, considering the role of CO in OH reactivity. From 2006 to 2017, the average
530 OH reactivity of CO at the LAN station exhibited a significant downward trend of -0.07 s⁻¹/yr ($\alpha =$
531 0.05 , $r = -0.80$) and dropped from 4.1 ± 0.7 s⁻¹ in 2006 to 3.0 ± 0.3 s⁻¹ in 2017.

532

533 **Data availability.** The data sources of number of fire emissions, the annual CO emissions and the
534 CO concentrations retrieved from MOPITT over the YRD region are all listed in the reference, and
535 the CO concentrations and the meteorological data at the LAN station can be inquired about by
536 contacting the corresponding author.

537 **Author contributions.** YJC, WLL, and BXX developed the idea for this paper and formulated the
538 research goals. QLM and JY carried out the CO field observations at the LAN station. WG provided
539 the CO data in Shanghai. YJC and WLL wrote and revised the manuscript with contributions from
540 all co-authors.



541 **Competing interests.** The authors declare that they have no conflict of interest.

542 **Acknowledgments.** This study was funded by the National Key R&D Program of China
543 (2016YFC0201900), National Natural Science Foundation of China (91744206), and Beijing
544 Science and Technology program (Z181100005418016). We thank the personnel on duty at the LAN
545 station for their assistance. This manuscript was edited by Wallace Academic Editing.

546 **References**

- 547 Ahmed, E., Kim, K.H., Jeon, E.C., Brown, R.J.C., 2015. Long term trends of methane, non-
548 methane hydrocarbons, and carbon monoxide in urban atmosphere. *Science of the Total*
549 *Environment* 518, 595-604.
- 550 Andreae, M., Merlet, P., 2001. Emission of trace gases and aerosols from biomass burning.
551 *Global Biogeochemical Cycles*, v.15, 955-966 (2001) 15.
- 552 Bakwin P S, Tans P P, Novelli P., 1994. CO budget in the Northern Hemisphere. *Geophys Res*
553 *Lett*, 21:433-436.
- 554 Crutzen, P.J., Heidt, L.E., Krasnec, J.P., Pollock, W.H., Seiler, W., 1979. Biomass burning as a
555 source of atmospheric gases CO, H₂, N₂O, NO, CH₃Cl and COS. *Nature* 282, 253-256.
- 556 Cohen, Y., Petetin, H., Thouret, V., Marecal, V., Josse, B., Clark, H., Sauvage, B., Fontaine, A.,
557 Athier, G., Blot, R., Boulanger, D., Cousin, J.M., Nedelec, P., 2018. Climatology and long-
558 term evolution of ozone and carbon monoxide in the upper troposphere-lower stratosphere
559 (UTLS) at northern midlatitudes, as seen by IAGOS from 1995 to 2013. *Atmos Chem*
560 *Phys*, 18: 5415-5453.
- 561 Daniel J S, Solomon S. On the climate forcing of carbon monoxide. *Journal of Geophysical*
562 *Research*, 1998, 103(D11): 13249-13260.
- 563 Deeter, M., Edwards, D., Francis, G., Gille, J., Martínez-Alonso, S., Worden, H., Sweeney, C.,
564 2017. A climate-scale satellite record for carbon monoxide: The MOPITT Version 7
565 product. *Atmos Meas Tech* 10, 2533-2555.
- 566 Di Carlo, P., Brune, W.H., Martinez, M., Harder, H., Leshner, R., Ren, X., Thornberry, T., Carroll,
567 M.A., Young, V., Shepson, P.B., Riemer, D., Apel, E., Campbell, C., 2004. Missing OH
568 Reactivity in a Forest: Evidence for Unknown Reactive Biogenic VOCs. *Science* 304, 722.
- 569 Fang S, Zhou L, Luan T., et al. Distribution of CO at Lin'an Station in Zhejiang Province.
570 *ENVIRONMENTAL SCIENCE*, 2014, 35(7): 2454-2459.
- 571 Gao W, Tie X, Xu J, et al. Long-term trend of O₃, in a mega City (Shanghai), China:
572 Characteristics, causes, and interactions with precursors. *Science of The Total*
573 *Environment*, 2017, 603-604: 425-433.
- 574 Global Atmosphere Watch Programme/ The World Data Centre for Greenhouse Gases
575 (WDCGG) <https://gaw.kishou.go.jp/>
- 576 Hao, N., Valks, P., Loyola, D., Cheng, Y.F., Zimmer, W., 2011. Space-based measurements of
577 air quality during the World Expo 2010 in Shanghai. *Environmental Research Letters* 6,
578 044004.
- 579 Holloway T, Levy II H, Kasibhatla P. Global distribution of carbon monoxide. *Journal of*



- 580 Geophysical Research, 2000, 105(D10): 12123-12147.
- 581 Huang X, Huang X, Wang T, et al. Observation and analysis of urban upper atmospheric carbon
582 monoxide in Nanjing. *China Environmental Science*, 2013a, 33(9).
- 583 Huang Y, Wei H, Duan Y, et al. Ambient Air Quality Status and Reason Analysis of Shanghai
584 World Expo. *Environmental Monitoring in China*, 2013b, 29(5).
- 585 Ingham, T., Goddard, A., Whalley, L.K., Furneaux, K.L., Edwards, P.M., Seal, C.P., Self, D.E.,
586 Johnson, G.P., Read, K.A., Lee, J.D., Heard, D.E., 2009. A flow-tube based laser-induced
587 fluorescence instrument to measure OH reactivity in the troposphere. *Atmos. Meas. Tech.*
588 2, 465-477.
- 589 Khalil M A K, Rasmussen R A. The global cycle of carbon monoxide: trends and mass balance.
590 *Chemosphere*, 1990,20:227-242.
- 591 Kovacs, T., Brune, W., 2001. Total OH Loss Rate Measurement. *Journal of Atmospheric*
592 *Chemistry* 39, 105-122.
- 593 Lei, Y., Zhang, Q., Nielsen, C.P., He, K.B., 2011. An inventory of primary air pollutants and
594 CO₂ emissions from cement industry in China, 1990-2020. *Atmospheric Environment* 45,
595 147-154.
- 596 Li, M., Zhang, Q., Kurokawa, J., Woo, J., He, K., Lu, Z., Ohara, T., Song, Y., Streets, D.G.,
597 Carmichael, G.R., Cheng, Y., Hong, C., Huo, H., Jiang, X., Kang, S., Liu, F., Su, H., and
598 Zheng, B., MIX: a mosaic Asian anthropogenic emission inventory under the international
599 collaboration framework of the MICS-Asia and HTAP, *Atmos. Chem. Phys.*, 17, 935–963,
600 2017.
- 601 Lin H, Wang Y, Hu B, et al. Observation and research on carbon monoxide in the atmosphere
602 of Beijing during the summertime of 2007. *Environmental Chemistry*, 2009, 28(4) : 567-
603 570.
- 604 Lin W, Xu X, Sun J, et al. Study of the background concentrations of reactive gases at Jinsha
605 regional atmospheric background station and the impacts of long-range transport. *Sci*
606 *ChinaEarth*, 2011, 54(10): 1604-1613.
- 607 Lin W, Xu X, Yu D, et al. Quality Control for Reactive Gases Observation at Longfengshan
608 Regional Atmospheric Background Monitoring Station, *Meteorological Monthly*, 35(11):
609 93-100,2009.
- 610 Lin W, Xu X, Zhang X. The errors in the claimed concentrations of standard gases used in the
611 observation of reactive gases and recommended solutions. *Environmental Chemistry*.
612 30(6): 1-4, 2011.
- 613 Lin, W., Xu, X., Sun, J., Liu, X., Wang, Y., 2011. Background concentrations of reactive gases
614 and the impacts of long-range transport at the Jinsha regional atmospheric background
615 station. *Science China Earth Sciences* 54, 1604-1613.
- 616 Liu, S., Fang, S.X., Liang, M., Sun, W.Q., Feng, Z.Z., 2019. Temporal patterns and source
617 regions of atmospheric carbon monoxide at two background stations in China. *Atmos Res*
618 220, 169-180.
- 619 Lou, S., F, H., F, R., Lu, K., B, B., Brauers, T., Chang, C.C., H, F., Häsel, R., Kita, K., Y, K.,
620 Li, X., M, S., Zeng, L., A, W., Zhang, Y., Wang, W., A, H., 2009. Atmospheric OH
621 reactivities in the Pearl River Delta - China in summer 2006: Measurement and model
622 results. *Atmospheric Chemistry and Physics Discussions* 10.
- 623 Martinerie P, Brasseur G P, Granier C. The chemical composition of ancient atmospheres-a



- 624 model study constrained by ice core data. *Journal of Geophysical Research*, 1995, 100
625 (D7): 14291-14304
- 626 Meng Z, Ding G, Tang J, et al. Characteristics of Trace Gases at Shangdianzi Background
627 Station in Autumn and Winter in Beijing. *Meteorological science and technology*, 2007,
628 35(4):550-557.
- 629 Meng Z. Y.*, Lin W. L., Wang S. F. et al. Characteristics of trace gaseous pollutants at a regional
630 background station in Northern China. *Atmos. Chem. Phys.*, 9: 927-936, 2009.
- 631 Meng, Z.Y., Xu, X.B., Yan, P., Ding, G.A., Tang, J., Lin, W.L., Xu, X.D., Wang, S.F., 2009.
632 Characteristics of trace gaseous pollutants at a regional background station in Northern
633 China. *Atmos Chem Phys* 9, 927–936.
- 634 MOPITT (Measurements of Pollution in the Troposphere) Version 8 Product User's Guide,
635 [https://www2.acom.ucar.edu/sites/default/files/mopitt/v8_users_guide_201812.pdf?_ga=2.33](https://www2.acom.ucar.edu/sites/default/files/mopitt/v8_users_guide_201812.pdf?_ga=2.33903080.811721902.1572782618-1653752621.154823800)
636 [903080.811721902.1572782618-1653752621.154823800](https://www2.acom.ucar.edu/sites/default/files/mopitt/v8_users_guide_201812.pdf?_ga=2.33903080.811721902.1572782618-1653752621.154823800)
- 637 Novelli P C, Steele P L, Tans P P. Mixing ratios of carbon monoxide in the troposphere. *Journal*
638 *of Geophysical Research*, 1992, 97(D18): 731-750.
- 639 Novelli P C, Masarie K A, Lang P M. Distributions and recent changes of carbon monoxide in
640 the lower troposphere. *Journal of Geophysical Research*, 1998, 103(D5): 19015-19033.
- 641 N. Türkoglu, I. Çiçek, G. Gürgen. Analysis of effects of meteorological factors on air pollutant
642 concentrations in Ankara, Turkey. *Il Nuovo Cimento C*, 2004, 27(4):14-14.
- 643 Petrenko V V, Martinerie P, Novelli P, et al. A 60 yr record of atmospheric carbon monoxide
644 reconstructed from Greenland firn air. *Atmospheric Chemistry and Physics*, 2013, 13:
645 7567-7585.
- 646 Demerjian K, Alistairkerr J, Calvert J. The Predicted Effect of Carbon Monoxide on the Ozone
647 Levels in Photochemical Smog Systems. *Environmental Letters*, 1972, 3(2):73-80.
- 648 Qi H X, Lin W L, Xu X B, et al. Significant downward trend of SO₂ observed from 2005 to
649 2010 at a background station in the Yangtze Delta region, China. *Science China Chemistry*,
650 2012, 55(7): 1451-1458.
- 651 Ren, X., Brune, W.H., Cantrell, C.A., Edwards, G.D., Shirley, T., Metcalf, A.R., Leshner, R.L.,
652 2005. Hydroxyl and Peroxy Radical Chemistry in a Rural Area of Central Pennsylvania:
653 Observations and Model Comparisons. *Journal of Atmospheric Chemistry* 52, 231-257.
- 654 Stein A F, Draxler R R, Rolph G D, et al. NOAA's HYSPLIT atmospheric transport and
655 dispersion modeling system. *Bulletin of the American Meteorological Society*,
656 2015:150504130527006.
- 657 Steinfeld, Jeffrey I. *Atmospheric Chemistry and Physics: From Air Pollution to Climate Change*.
658 *Environment Science & Policy for Sustainable Development*, 40(7): 26-26. 1998.
- 659 Thompson A M. The oxidizing capacity of the Earth's atmosphere: Probable past and future
660 changes. *Science*, 1992, 256(5060) : 1157-1165.
- 661 Thompson A M, Chappellaz J A, Fung I Y, et al. The atmospheric CH₄ increase since the Last
662 Glacial Maximum. *Tellus B*, 1993, 45(3).
- 663 Thompson A M, Cicerone R J. Possible perturbations to atmospheric CO, CH₄, and OH. *Journal*
664 *of Geophysical Research*, 1986, 91, (D10): 10853-10864.
- 665 Vukovich, F., 2000. Weekday/Weekend Differences in OH Reactivity with VOCs and CO in
666 Baltimore, Maryland. *Journal of the Air & Waste Management Association* (1995) 50,
667 1843-1851.



- 668 Wang, P., Elansky, N.F., Timofeev, Y.M., Wang, G., Golitsyn, G.S., Makarova, M.V., Rakitin,
669 V.S., Shtabkin, Y., Skorokhod, A.I., Grechko, E.I., Fokeeva, E.V., Safronov, A.N., Ran, L.,
670 Wang, T., 2018. Long-Term Trends of Carbon Monoxide Total Columnar Amount in
671 Urban Areas and Background Regions: Ground- and Satellite-based Spectroscopic
672 Measurements. *Adv Atmos Sci* 35, 785-795.
- 673 Werf, G., Randerson, J., Giglio, L., Leeuwen, T., Chen, Y., Rogers, B., Mu, M., Marle, M.v., Morton,
674 D., Collatz, G., Yokelson, R., Kasibhatla, P., 2017. Global fire emissions estimates during
675 1997-2016. *Earth System Science Data* 9, 697-720. data source:
676 <https://www.geo.vu.nl/~gwerf/GFED/GFED4/>.
- 677 Worden, H.M., Deeter, M.N., Frankenberg, C., George, M., Nichitiu, F., Worden, J., Aben, I.,
678 Bowman, K.W., Clerbaux, C., Coheur, P.F., de Laat, A.T.J., Detweiler, R., Drummond,
679 J.R., Edwards, D.P., Gille, J.C., Hurtmans, D., Luo, M., Martínez-Alonso, S., Massie, S.,
680 Pfister, G., Warner, J.X., 2013. Decadal record of satellite carbon monoxide observations.
681 *Atmos Chem Phys*, 13, 837-850.
- 682 WMO. World Data Center for Greenhouse Gases Data Summary. Tokyo, Japan, WMO
683 WDCGG Report, 2003, 27:1-92.
- 684 Wu Y, Xu H, Y D. Characteristics of CO concentrations at the Longfengshan regional
685 background station. *Environmental Chemistry*, 2008, 27(6) : 847-848.
- 686 Xue M, Wang Y, Sun Y. Measurement on the Atmospheric CO Concentration in Beijing.
687 *Environmental Science*, 2006, 27(2) : 200-206.
- 688 Xia, L., Zhou, L., Tans, P., Liu, L., Wang, H., Luan, T., Zhang, G., 2015. Atmospheric CO₂ and
689 its δ¹³C measurements from flask sampling at Lin'an regional background station in
690 China. *Atmospheric Environment* 117.
- 691 Yan X, Ohara T, Akimoto H . Bottom-up estimate of biomass burning in mainland China.
692 *Atmospheric Environment*, 2006, 40(27):5262-5273.
- 693 Yang J, Liu J, Yang G, et al. Characteristics and changing trend of carbon monoxide pollution
694 in Tianjin. *Environmental science and management*, 2012, 37(6): 89-104.
- 695 Yang D, Yu X, Li X. Distribution characteristics of trace gas concentrations at the Lin 'an
696 background station and the effect on aerosols. *Journal of applied meteorology*, 1995,
697 6(4):400-406.
- 698 Ye F, An J, Wang Y, et al. Analysis of O₃, NO_x, CO and correlation meteorological factor at the
699 ground layer in Beijing. *Ecology and Environment*, 2008(4):115-122.
- 700 Yurganov, L., McMillan, W., Grechko, E., Dzhola, A., 2010. Analysis of global and regional
701 CO burdens measured from space between 2000 and 2009 and validated by ground-based
702 solar tracking spectrometers. *Atmos Chem Phys* 10, 3479-3494.
- 703 Zhang F, Zhou L X, Novelli P C, et al. Evaluation of in situ measurements of atmospheric
704 carbon monoxide at Mount Waliguan, China. *Atmospheric Chemistry Physics*, 2011,
705 11(11) : 5195-5206.
- 706 Zhang, G., Xu, H., Qi, B., Du, R., Gui, K., Wang, H., Jiang, W., Liang, L., and Xu, W.:
707 Characterization of atmospheric trace gases and particulate matter in Hangzhou, China,
708 *Atmos. Chem. Phys.*, 2018, 1705-1728.
- 709 Zhang L, Fu C, Zheng X, et al. Analysis of air pollution characteristics and influencing factors
710 in urban areas of Guangzhou. *Ecology and Environment*, 2007, 16(2): 305-308.
- 711 Zhou L, Wen Y, Li J, et al. Background variation in atmospheric carbon monoxide at



- 712 Mt. Waliguan, China. *Acta Scientiae circumstantiae*, 2004, 24(4): 637-642.
- 713 Zhao, H., Zheng, Y.F., Wei, L., Guan, Q., Wang, Z.S., 2017. Evolution and evaluation of air
714 quality in Hangzhou and its surrounding area during the G20 summit. *China*
715 *Environmental Science*, 37, 2016-2024.
- 716 Zhao, Y., Wang, S.X., Duan, L., Lei, Y., Cao, P.F., Hao, J.M., 2008. Primary air pollutant
717 emissions of coal-fired power plants in China: current status and future prediction.
718 *Atmospheric Environment* 42, 8442-8452.
- 719 Zhao Y, Nielsen C P, Mcelroy M B, et al. CO emissions in China: Uncertainties and implications
720 of improved energy efficiency and emission control. *Atmospheric Environment*, 2012,
721 49:103-113.
- 722 《Ambient air quality standard 》(GB 3095-2012), Ministry of ecology and environment, PRC.
723 http://kjs.mee.gov.cn/hjbhzb/bzwb/dqhjbh/dqhjzlbz/201203/t20120302_224165.shtml
- 724 Action plan for the prevention and control of air pollution of the People's Republic of China.
725 http://www.gov.cn/zhengce/content/2013-09/13/content_4561.htm
- 726 Zhu L, Wang G, Zhang Y. Spatial and temporal distribution characteristics of the crop straw
727 resources in the Yangtze river delta region. *Agricultural science of Guizhou*, 2017(4).